An Exciplex-Based Light-Emission Pathway for Solution-State Electrochemiluminescent Devices

Chang-Ki Moon, Julian F. Butscher, and Malte C. Gather*

Electrochemiluminescence (ECL) allows the design of unique light-emitting devices that use organic semiconductors in a liquid or gel state, which allows for simpler and more sustainable device fabrication and facilitates unconventional device form-factors. Compared to solid-state organic LEDs, ECL devices (ECLDs) have attracted less attention due to their currently much lower performance. ECLD operation is typically based on an annihilation pathway that involves electron transfer between reduced and oxidized luminophore species; the intermediate radical ions produced during annihilation dramatically reduce device stability. Here, the effects of radical ions are mitigated by an exciplex formation pathway and a remarkable improvement in luminance, luminous efficacy, and operational lifetime is demonstrated. Electron donor and acceptor molecules are dissolved at high concentrations and recombined as an exciplex upon their oxidization/reduction. The exciplex then transfers its energy to a nearby dye, allowing the dye to emit light without undergoing oxidation/reduction. Furthermore, the application of a mesoporous TiO_2 electrode increases the contact area and hence the number of molecules participating in ECL, thereby obtaining devices with a very high luminance of 3790 cd m^{-2} and a 30-fold improved operational lifetime. This study paves the way for the development of ECLDs into highly versatile light sources.

1. Introduction

Electrochemiluminescence (ECL) allows the generation of light from organic molecules dissolved in a liquid or gel that is positioned between two electrodes.[1] The sensitivity and selectivity of ECL to different ions have led to the development of a range of chemosensors, biosensors, immunoassays, and environmental detectors.[2] In addition, liquid-type ECL devices (ECLDs) can be fabricated in an extremely facile manner by simply injecting a liquid through a microfluidic channel into a pre-fabricated cell with opposite electrodes. This enables miniaturized devices and on-demand reconfiguration of the device form factor,[2d,3] lowers process costs, and reduces material wastage during manufacturing compared to the solid-state counterpart of the ECLD, the organic light-emitting diode (OLED). However, in contrast to OLEDs, ECLDs have attracted less attention for display and lighting applications because of their relatively low light output and stability.

Most ECLDs reported to date operate based on an annihilation pathway that involves redox reactions of the luminophores and subsequent electron transfer between reduced and oxidized luminophore species to generate excitons. Coreactants can also be involved in these redox or electron-transfer reactions.[1c,d] Work to improve the performance of ECLDs has included different aspects of material development[4] and device operation.[1c,5] For instance, AC operation, possibly combined with an optimized input waveform,[5c,d] offers higher performance and a faster turn-on response than DC operation since the diffusion lengths of molecular ions in the ECL liquid are too short to allow the ions to travel across the gap between the two electrodes (which is typically in the range of tens to hundreds of μm).[5a,b] Despite many efforts, the highest luminance reported for liquid- or gel-type ECLDs so far is only 700 cd m^{-2}.[1c] Moreover, operational lifetimes under continuous operation are rarely reported and remain limited to the second or minute range at best.[1a,4d,6] Therefore, to the best of our knowledge, ECLDs have not yet found practical applications as photonic devices and any future use will require a systematic improvement of their luminance and operational stability.

It has been hypothesized that the annihilation pathway on which current ECLDs operate entails a number of parasitic side reactions, which start from intermediate reduced or oxidized luminophore species and ultimately lead to the loss of emissive molecules in the device or the formation of dark states.[1d] In addition, increasing the luminophore concentration beyond a cer-

C.-K. Moon, J. F. Butscher, M. C. Gather
Humboldt Centre for Nano- and Biophotonics
Department of Chemistry
University of Cologne
Greinstr. 4–6, 50939 Köln, Germany
E-mail: mcg6@st-andrews.ac.uk
C.-K. Moon, J. F. Butscher, M. C. Gather
Organic Semiconductor Centre
School of Physics and Astronomy
University of St Andrews
North Haugh, St Andrews KY16 9SS, UK

**ADVANCED
SCIENCE NEWS**

www.advancedsciencenews.com
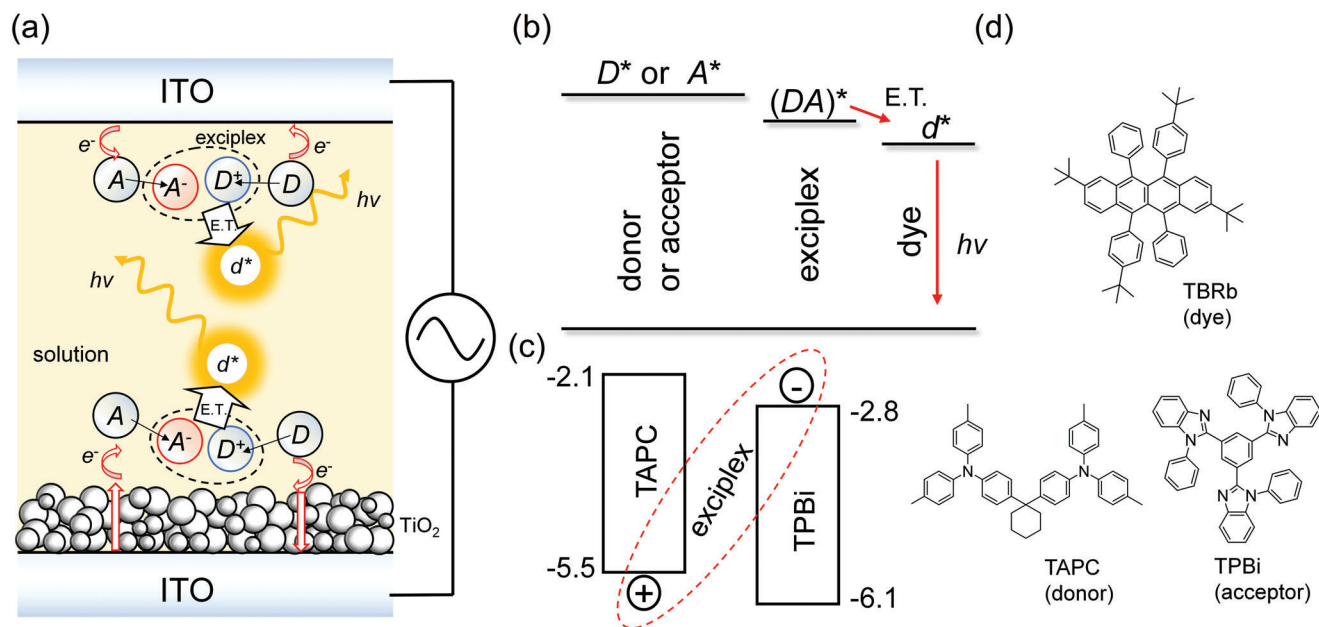
**ADVANCED
MATERIALS**

www.advmat.de

Figure 1. Illustration of how electrochemiluminescence (ECL) can be achieved via an exciplex formation pathway. a) Schematic illustration of an ex-ECLD. Under AC operation, the donor (*D*) and acceptor (*A*) molecules dissolved in the solution are alternately oxidized and reduced at both the TiO₂ electrode and the ITO electrode. Upon collision, oxidized donors and reduced acceptors form exciplexes. The exciplex transfers its energy to a neighboring dye molecule (*d*) via resonant energy transfer (E.T.), ultimately leading to emission from the dye molecule. The mesoporous TiO₂ electrode increases the effective contact area and thus promotes the redox reaction. b) Summary of the energy levels of the excited singlet states of the donor, acceptor, exciplex, and dye. c) Illustration of how exciplex formation is enabled by the staggered HOMO/LUMO energy levels of TAPC and TPBi. The values shown for the HOMO and LUMO levels are taken from ref. [9]. d) Chemical structures of TAPC, TPBi, and TBRb.
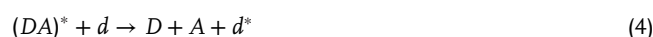
tain concentration does not further improve the rate of ECL due to self-absorption and luminescence quenching.

Here, we introduce a solution to mitigate the issues outlined above based on the use of exciplex states. Our approach improves the efficiency of ECL reactions and at the same time minimizes the rate at which parasitic side reactions occur. Exciplexes are formed by bimolecular recombination between different oxidized and reduced species. The use of exciplexes has become a popular strategy for improving charge carrier injection and charge recombination in OLEDs in recent years.[7] As exciplex formation via long-range coupling between organic semiconductor ions has been observed in diluted and spatially-separated films,[8] we hypothesize that efficient exciplex formation can also be achieved in solution. The light-emission pathway in our devices is based on the formation of exciplexes via recombination between oxidized electron donors and reduced electron acceptor molecules that are generated by application of an AC bias. Following exciplex formation, energy is then transferred to nearby dye molecules for efficient luminescence. This operating mechanism improves the reliability of the ECL reactions by spatially separating ionization/recombination from light emission. This approach also improves the likelihood and thus, the efficiency, of ionization/recombination as high concentrations of donor and acceptor molecules can be present without causing a loss of efficiency due to self-absorption and luminescence quenching. We demonstrate that compared to conventional ECLDs, exciplex ECLDs (ex-ECLDs) exhibit improved luminance, luminous efficacy, switching speed, and operational lifetime. Further improvements are achieved via the application of a mesoporous TiO₂ elec-

trode that increases the effective contact area. An optimized ex-ECLD with a TiO₂ electrode reaches a maximum total luminance of up to 3790 cd m⁻², with 2260 cd m⁻² emitted through the ITO electrode and 1530 cd m⁻² through the TiO₂ electrode. Operational lifetime studies reveal lifetime acceleration factors of less than 1 due to the increase in efficiency of our ex-ECLDs with increasing luminance. At an initial brightness of 300 cd m⁻², ex-ECLDs with and without a TiO₂ electrode achieve LT₅₀ lifetimes of 35 and 312 s, respectively. These values represent 3-fold and nearly 30-fold improvements over the 11-s lifetime of conventional ECLDs.

2. Results and Discussion

Figure 1a schematically illustrates the operating mechanism of our ex-ECLD. The ECL solution consists of an electron-donor molecule (*D*), an electron-acceptor molecule (*A*), a dye (*d*), a solvent, and a supporting electrolyte. During device operation, we expect the following reactions to occur
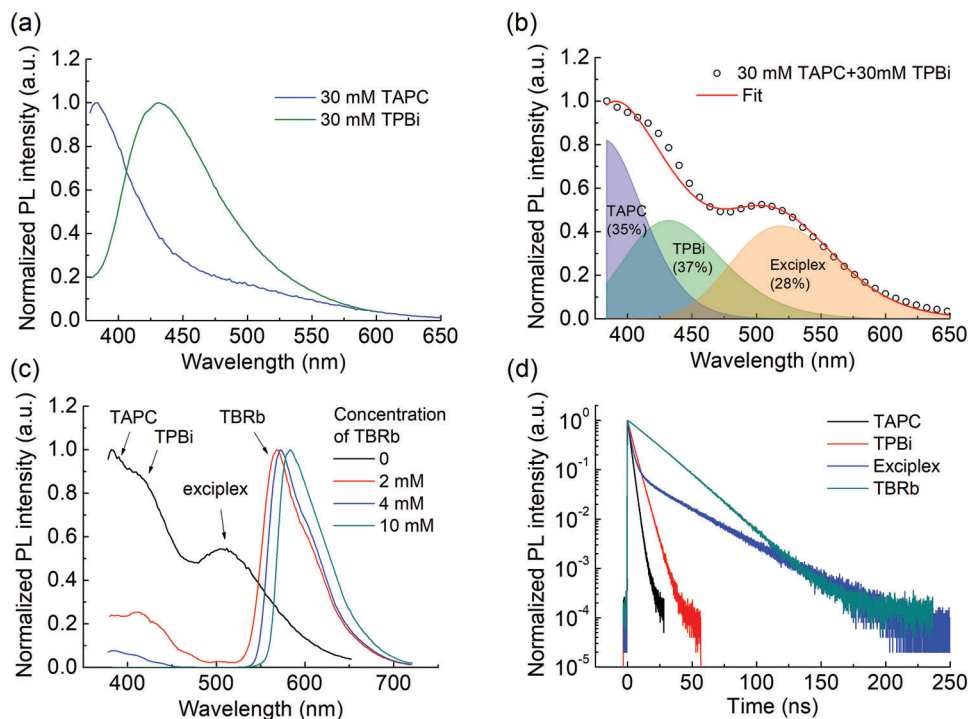
$$D \rightarrow D^+ + e^- \tag{1}$$

$$A + e^- \rightarrow A^- \tag{2}$$

$$D^+ + A^- \rightarrow (DA)^* \tag{3}$$

$$(DA)^* + d \rightarrow D + A + d^* \tag{4}$$

$$d^* \rightarrow d + h\nu \tag{5}$$

**ADVANCED
SCIENCE NEWS**

www.advancedsciencenews.com

**ADVANCED
MATERIALS**

www.advmat.de

Figure 2. PL measurements to investigate exciplex formation and energy transfer in the solutions used for ECL. a) PL spectra for 3×10^{-2} M TAPC and 3×10^{-2} M TPBi solutions, respectively. b) PL spectrum of a mixture of 3×10^{-2} M TAPC and 3×10^{-2} M TPBi (open circles). The PL spectrum was deconvoluted into three Gaussian energy distributions associated with emission from TAPC ($\mu_1 = 3.25$ eV, mean, and $\sigma_1 = 0.24$ eV, standard deviation), TPBi ($\mu_2 = 2.87$ eV and $\sigma_2 = 0.25$ eV), and the exciplex ($\mu_3 = 2.39$ eV and $\sigma_3 = 0.19$ eV). c) PL spectra for solutions of 3×10^{-2} M TAPC and 3×10^{-2} M TPBi containing different concentrations of TBRb. d) Transient PL decay for pure solutions of TAPC and TPBi, for the exciplex emission peak in the TAPC:TPBi mixture, and for the TBRb emission peak in the TAPC:TPBi:TBRb mixture. The fluorescence lifetimes of TAPC, TPBi, and TBRb are 2.23, 4.24, and 20.8 ns, respectively. The exciplex exhibits prompt and delayed fluorescence with lifetimes of 2.45 and 27.4 ns, respectively.

Under AC operation, the donor and acceptor are alternately oxidized and reduced at either electrode (Equations (1) and (2)). The donor cation and acceptor anion are then electrostatically attracted to each other and recombine forming the exciplex $(DA)^*$ (Equation (3)). The dye is subsequently excited via Förster resonance energy transfer (FRET) from the exciplex (Equation (4)) and finally emits a photon by radiative relaxation (Equation (5)). A thin mesoporous TiO$_2$ electrode can be coated onto the surface of one of the electrodes (see below). Figure 1b shows the energy level alignment required for efficient ex-ECLD operation for the simpler singlet case, with the dye molecules having the lowest singlet energy level, thereby forming the terminal emitter. Both the donor and acceptor have higher singlet energy levels than the exciplex to avoid energy back-transfer. In addition, the donor must possess higher HOMO and LUMO levels than the acceptor (type-II heterojunction) to allow exciplex formation, as depicted in Figure 1c.

The proposed mechanism offers many benefits for device operation. First, it suppresses the degeneration of the dye by avoiding repeated redox reactions involving the dye. Second, the concentration of the dye in the ECL solution can be kept lower, thus avoiding self-absorption; instead, high concentrations of the donor and acceptor molecules are used to increase the probability of reduction/oxidization and ion collision and, hence, exciplex formation. Thirdly, the electrical generation of the exciplex offers faster and longer-range coupling between the molecular

ions than the annihilation pathway used in conventional ECLDs because our exciton-based mechanism does not require electron transfer between the molecules.

In this study, we chose 1,1-bis[(di-4-tolylamino)phenyl]cyclohexane (TAPC) and 2,2′,2″-(1,3,5-benzinetriyl)-tris(1-phenyl-1-H-benzimidazole) (TPBi, energy levels and chemical structures are shown in Figures 1c,d, respectively) as the donor and acceptor, respectively. The exciplex between TAPC and TPBi was previously investigated in mixed films,[9] but to our knowledge, has not yet been analyzed in solution. Yellow-emissive 2,8-di-*tert*-butyl-5,11-bis(4-*tert*-butylphenyl)-6,12-diphenyltetracene (TBRb, chemical structure shown in Figure 1d) was chosen as the dye for the ECL solution. To solubilize both neutral molecules and the ion radicals formed under application of voltage, we used a 2:1 (by volume) mixture of toluene and acetonitrile as the solvent (i.e., a less polar and a more polar solvent, respectively).[4a]

The PL spectra of pure TAPC and TPBi solutions have emission peaks at 384 and 432 nm, respectively (**Figure 2**a). However, a solution containing both TAPC and TPBi at 3×10^{-2} M exhibited an additional, red-shifted emission peak, indicating the presence of a TAPC:TPBi exciplex (Figure 2b). Deconvoluting the spectrum of the mixture with Gaussian energy distributions for emission from TAPC, TPBi, and the exciplex placed the exciplex emission peak at 518 nm and shows that this peak represents 28% of the total emission intensity. Even when only a

**ADVANCED
SCIENCE NEWS**

www.advancedsciencenews.com

**ADVANCED
MATERIALS**

www.advmat.de

relatively small amount of TBRb (2×10^{-3} M) was added to the TAPC:TPBi mixture, the emission spectrum became dominated by TBRb emission (Figure 2c) and the emission from TAPC, TPBi and the TAPC:TPBi exciplex was suppressed. When the concentration of TBRb reached 1×10^{-2} M, only emission from TBRb was observed with an emission peak at 583 nm. We attribute the rapid increase in TBRb emission with increasing concentration to the significant overlap between the emission spectrum of the exciplex and the absorption spectrum of TBRb (Figure S1, Supporting Information), which enables efficient FRET from the exciplex to TBRb.

To further confirm the presence of a TAPC:TPBi exciplex, we performed measurements of the transient PL upon picosecond optical excitation of the various solutions (Figure 2d). While a monoexponential PL decay was observed for the pure TAPC and TPBi solutions, the emission peak attributed to the exciplex in the PL spectrum of the mixture featured prompt and delayed emission components, with lifetimes of 2.45 and 27.4 ns, respectively. This bi-exponential decay is expected as the small energy gap between singlet and triplet excited states of the exciplex leads to efficient intersystem crossing (ISC) and reverse intersystem crossing (RISC).[10] The delayed fluorescence was observed only in the spectral range of exciplex emission and the emission by TPBi did not contribute to the delayed fluorescence (Figure S2a, Supporting Information). The emission from TBRb in the mixed TAPC:TPBi:TBRb solution exhibited a mono-exponential decay with a PL lifetime of 20.7 ns and the presence of the exciplex materials did not affect the PL lifetime of TBRb (Figure S2b, Supporting Information).

To fabricate functional ECLDs, 1×10^{-1} M of tetrabutylammonium hexafluorophosphate was added to the ECL solutions as a supporting electrolyte. Two different ECL solutions, one with and one without TAPC and TPBi, were used to create an ex-ECLD and a conventional ECLD, respectively. Devices were fabricated by spacing two ITO-coated glass substrates 30 μm apart and filling the gap with the respective solution (see the Experimental Section for details of device fabrication). **Figure 3**a shows a photograph of an ex-ECLD taken under ambient white light illumination with all four pixels turned on (pixel size, 2 mm × 2 mm each). The active area of each pixel is well-defined by sharp edges. The device is semitransparent with an orange hue stemming from the characteristic blue-to-green absorption of TBRb (for the TBRb absorption spectrum see Figure S1, Supporting Information). Figures 3b,c summarizes the transient ECL responses of the conventional ECLD and ex-ECLD, respectively, when driven with a square wave voltage with an amplitude of ±3.5 V and a frequency of 100 Hz. The conventional ECLD exhibited a smooth rise and decay in emission intensity after each change in applied voltage. The time to reach the peak emission intensity after switching voltage (t_{peak}) was 68 μs. By comparison, the switching speed of the ex-ECLD was faster ($t_{peak} = 30$ μs) and the peak emission intensity was higher than for the conventional ECLD, corroborating that the exciplex formation pathway leads to a faster and stronger ECL response than the conventional annihilation pathway since there is no interionic electron-transfer. In addition, two separate ECL intensity peaks were observed in the transient response of the ex-ECLD. We hypothesize that the first sharper peak represents faster, shorter-range coupling between molecular ions adjacent to the electrodes, and the second broader peak

originates from slower, longer-range coupling between the ions farther away from the electrodes.

To further characterize both ECLDs, we investigated their root-mean-square (rms) luminance (L_{rms}) under application of a sinusoidal voltage ($V_{rms} = 2.7$ V) with varying frequency (Figure 3d). The ex-ECLD exhibited higher luminance than the conventional ECLD across all investigated frequencies; the optimal frequencies were 302 and 268 Hz for the ex-ECLD and the ECLD, respectively. The optimal frequency is likely reached when there is a balance between the rate of redox reactions of the donor and acceptor molecules and the diffusion lengths for their ions to recombine under an electric field.[11] To enable a better comparison, Figures 3e,f depicts the rms current density–voltage (J_{rms}–V_{rms}) and rms luminance–voltage (L_{rms}–V_{rms}) characteristics, respectively, measured for both devices at a frequency of 300 Hz. Both ECLDs turned on at $V_{on} = 2.18$ V. Below V_{on}, the two devices show similar J_{rms}–V_{rms} curves because the current is governed by the non-faradaic contributions, including geometric capacitance and diffusion of electrolyte ions. Above V_{on}, the slope of J_{rms} versus V_{rms} increases sharply because the ECL reaction contributes to the current (faradaic current). The conventional ECLD then showed a drop in current density and luminance at around $V_{rms} = 2.9$ V. This coupled drop indicates that TBRb is responsible for both electric conduction and light emission in the conventional ECLD and that ionized TBRb molecules degrade during the annihilation pathway. By contrast, the ex-ECLD exhibited a continuous increase in luminance up to $V_{rms} = 3.40$ V without a drop in current density. This decoupling of current density and luminance indicates that TAPC and TPBi ions are responsible for electric conduction in the ex-ECLD and TBRb is only responsible for light emission in this device. The drop in luminance at high voltages is likely due to increasing side reactions by active solvents. As a result, the exciplex pathway increased the maximum achievable luminance from 390 to 1250 cd m^{-2}. Both devices had nearly identical emission spectra with an emission peak at 567 nm (Figure 3g), which demonstrates that while the exciplex pathway increases the concentration of TBRb excitons via efficient recombination and subsequent energy transfer processes, it does not impact the terminal part of the emission process. The luminous efficacy was also enhanced from 0.74 to 1.17 lm W^{-1} (Figure 3h, statistics of device performance in Figure S3, Supporting Information). Since ion collision is a second-order reaction, the rate of ion collision is proportional to the square of the ion concentration in the ECLD. Thus, at a high current density, molecular ions are more likely to emit light through the exciplex-formation pathway rather than return to neutral states through reverse oxidation/reduction reactions. This results in an increase in luminous efficacy as the luminance increases, at least up to the point where degeneration sets in.

The operational lifetime under prolonged AC operation (time until the luminance reduces to half of the initial value, LT_{50}) was found to be 78, 43, and 35 s for the ex-ECLD at an initial luminance of 100, 200, and 300 cd m^{-2}, respectively, whereas the corresponding LT_{50} of the conventional ECLD was only 26, 16, and 11 s (Figure 3i; the luminance decay curves over time are shown in Figures S4a,b, Supporting Information). The main cause of device degradation is presumed to be the chemical decomposition of TBRb based on the observation that the decrease in ECL intensity was larger than the decrease in the device current and
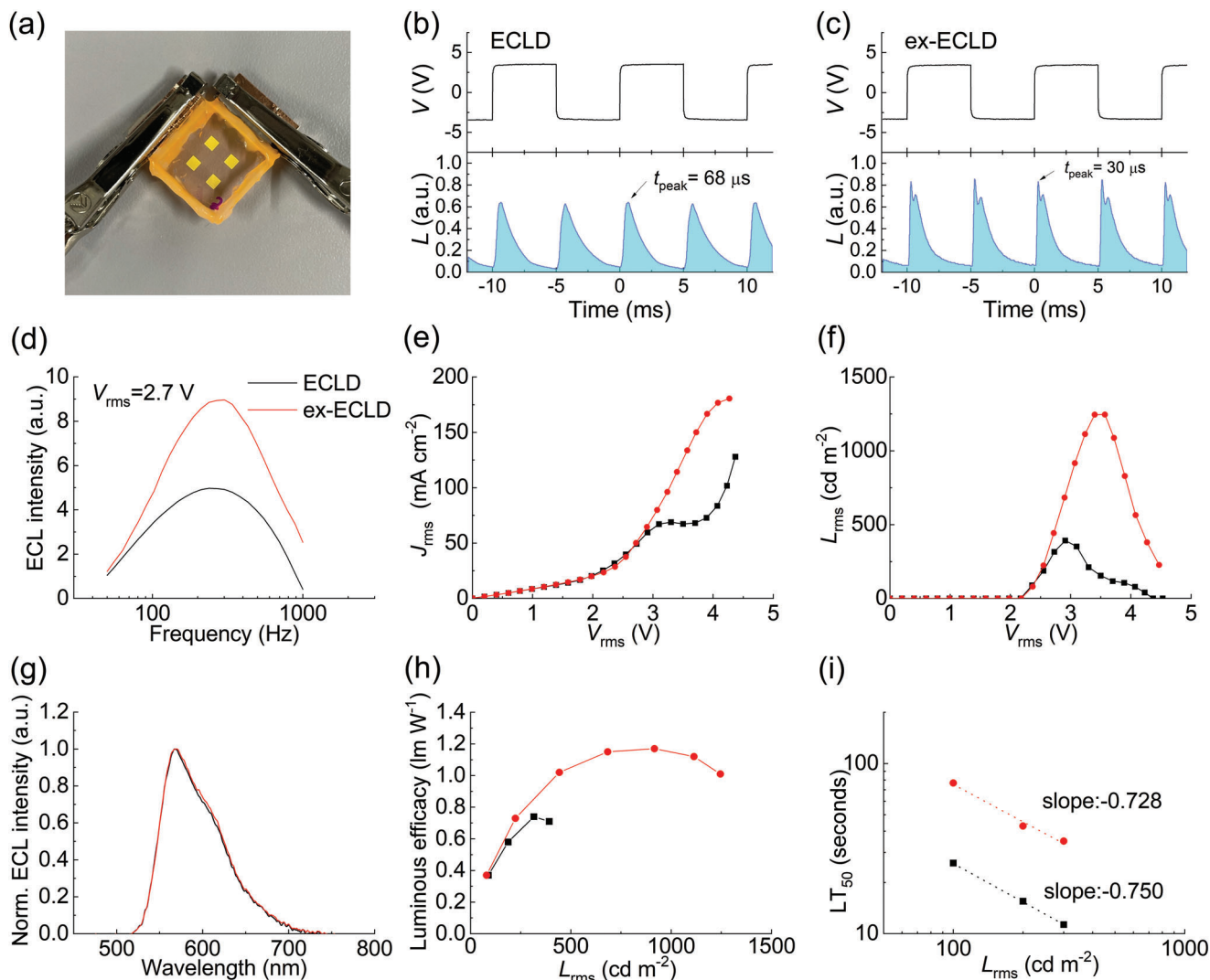
Figure 3. Device performance for conventional ECLD and ex-ECLD. a) Photograph of an ex-ECLD with all four emissive pixels turned on simultaneously. b) Transient response of a conventional ECLD under a square wave voltage signal with an amplitude of ± 3.5 V and a frequency of 100 Hz. c) Transient response of an ex-ECLD under the same operating conditions. d) Comparison of the emission intensity of a conventional ECLD and an ex-ECLD as a function of the frequency of a sinusoidal drive signal with $V_{rms} = 2.7$ V. e) Rms current density–voltage (J_{rms}–V_{rms}) characteristics. f) Rms luminance–voltage (L_{rms}–V_{rms}) characteristics. g) ECL spectra. h) Luminous efficacy versus L_{rms}. i) Operational lifetime (LT$_{50}$) versus initial L_{rms}. The dotted lines represent linear fits to log(LT$_{50}$) versus log(L_{rms}). Black and red lines and symbols correspond to the conventional ECLD and ex-ECLD, respectively. In (e) to (i), the devices were driven using a sinusoidal signal with a frequency of 300 Hz. The different ratio between the brightness of the conventional ECLD and the ex-ECLD in the frequency and voltage scans is attributed to different degradation of the two devices during the scans.

that the color of the active region of the cell was bleached by prolonged operation (Figures S4c,d, Supporting Information). The acceleration factors for the change in operational lifetime with initial luminance were found to be 0.728 and 0.750 for the ex-ECLD and the conventional ECLD, respectively; these values are below 1 due to the increase in efficiency conferred by the increase in luminance.

Note that although the emission produced by the ECLDs is in fact bidirectional, we only measured the emission in one direction in the luminance and lifetime analyses. Since the devices are symmetric, in theory, their luminance and luminous efficacy could be doubled by collecting photons emitted in both directions.

Next, to further improve device performance, we increased the contact area and promoted ionization at one of the ITO contacts by coating its surface with a mesoporous electrode composed of few-micrometer-sized grains of TiO$_2$.[12] **Figure 4**a shows a cross-section SEM image of the TiO$_2$ electrode laminated onto the ITO layer, indicating its effective thickness is 32 μm. Additional SEM images of different fields of view are presented in Figure S5, Supporting Information. The total optical transmittance of an identical TiO$_2$ electrode coated onto a glass substrate, as measured with an integrating sphere collecting both directly transmitted and diffusely transmitted light, ranged from 35% to 41% in the spectral region of TBRb emission ($\lambda = 550$ nm to 700 nm, Figure 4b).
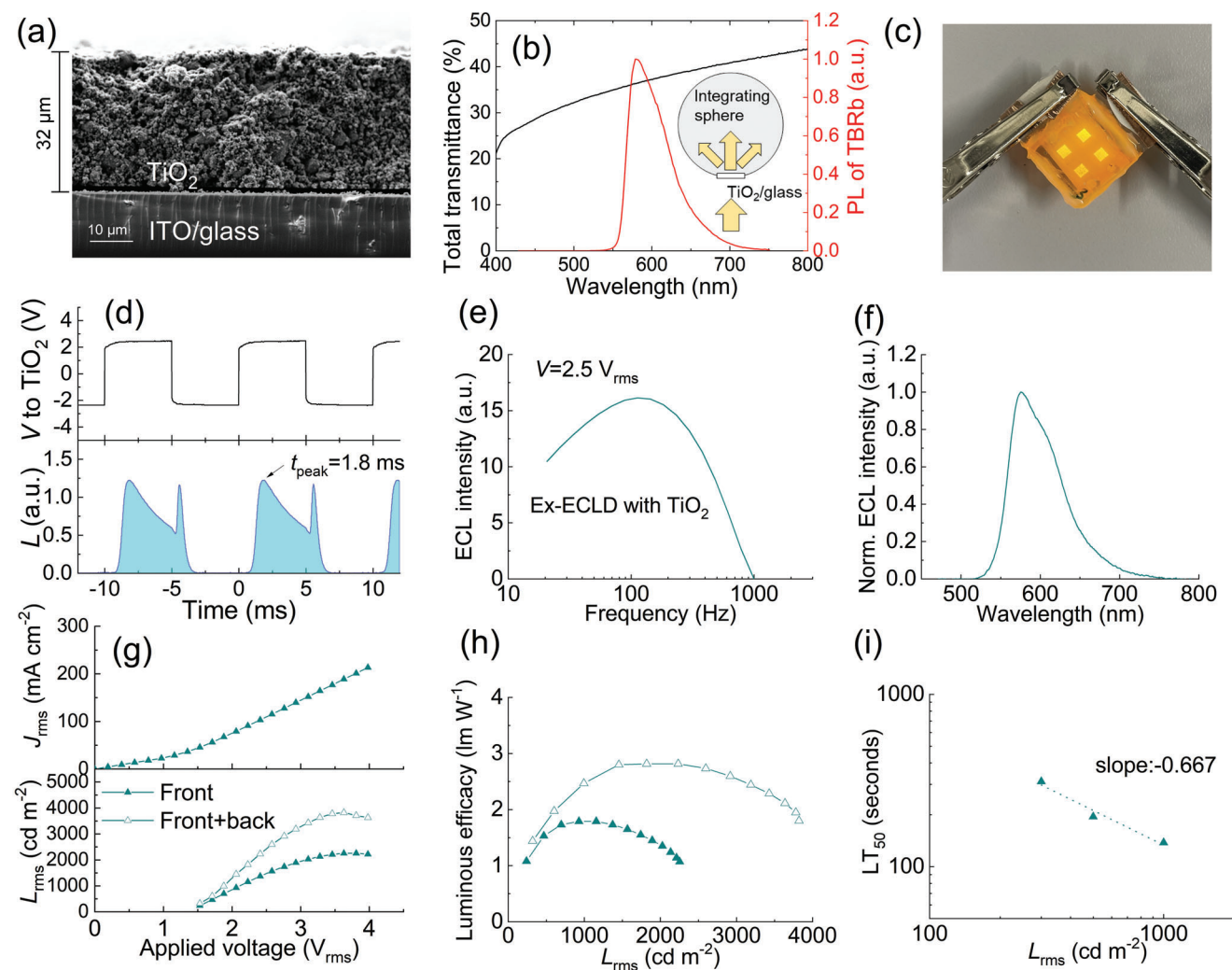
Figure 4. Device performance for ex-ECLDs with a TiO$_2$ electrode. a) Cross-section SEM image of a TiO$_2$ electrode laminated onto an ITO-coated glass substrate. b) Total optical transmittance of a TiO$_2$ electrode coated onto a glass substrate (black line) and photoluminescence spectrum of the TBRb emitter (red line). The inset illustrates the integrating sphere setup used for the measurements. c) Photograph of an ex-ECLD with a TiO$_2$ electrode with all four emissive pixels turned on simultaneously. The pixels have blurry edges due to light scattering by the mesoporous TiO$_2$. d) Transient ECL response under the application of a square wave voltage with an amplitude of ±2.5 V and a frequency of 100 Hz. e) Emission intensity versus frequency for a sinusoidal drive signal with V_{rms} = 2.7 V. f) ECL spectrum. g) Current density–voltage–luminance (J_{rms}–V_{rms}–L_{rms}) characteristics. h) Luminous efficacy versus L_{rms}. i) Operational lifetime (LT$_{50}$) versus initial L_{rms}. The dotted line represents a linear fit to log(LT$_{50}$) versus log(L_{rms}). In (f) to (i), the devices were driven using a sinusoidal signal with a frequency of 300 Hz.

Figure 4c shows a photograph of an ex-ECLD fabricated with a TiO$_2$ electrode coated onto one of the ITO-coated glass substrates. For this device, the emissive pixels have blurry edges due to the presence of significant light scattering in the TiO$_2$ electrode. Figure 4d shows the transient ECL response under the application of a square voltage signal with an amplitude of ±2.5 V and a frequency of 100 Hz. Compared to the symmetric ex-ECLD, the introduction of the TiO$_2$ electrode on one electrode resulted in an asymmetric transient ECL response, where the positive voltage pulse applied to the TiO$_2$ electrode was associated with a much slower decay in ECL than the negative half cycle, consistent with results reported by Okamoto et al. for a different system.[11c] We expect most ECL to occur near the TiO$_2$ electrode rather than near the opposite bare ITO electrode due to the larger contact area

of the TiO$_2$ electrode. Asymmetric ECL has previously been interpreted as a sign of an imbalance in the ion concentrations.[5c] For the operation of our ex-ECLDs, we assume that the electron transfer through the conduction band of TiO$_2$ facilitates the reduction of TPBi more than the oxidation of TAPC.[11b,c] When a negative voltage is applied to the TiO$_2$ electrode, TPBi anions accumulate near the TiO$_2$ electrode. The subsequent application of a positive potential generates TAPC cations, thus allowing ECL via the exciplex formation pathway. ECL continues until the next reversal of voltage, after 5 ms, due to the relatively slow generation of TAPC cations. The relatively lower rate of TAPC cation generation also means that only a small number of anions accumulate in the solution during the positive half cycle. Upon switching back to a negative voltage, TPBi anions are again generated at a high rate,

**ADVANCED
SCIENCE NEWS**

www.advancedsciencenews.com

**ADVANCED
MATERIALS**

www.advmat.de

and quickly consume any accumulated TAPC cations and thus lead to faster ECL decay during this half cycle.

The ex-ECLDs with a TiO$_2$ electrode were further characterized when driven with a sinusoidal voltage. Compared to the symmetric ex-ECLD with two ITO electrodes, the optimal operating frequency was downshifted from 302 Hz to 144 Hz by the TiO$_2$ electrode (Figure 4e), which agrees well with the slower switching speed ($t_{peak} = 1.8$ ms) observed for its transient ECL response. To enable a fair comparison with previously demonstrated devices, we analyzed the device characteristics at the same drive frequency of 300 Hz. The TiO$_2$ electrode caused a slight redshift of the emission spectrum to a peak emission wavelength of 575 nm (Figure 4f). In the J_{rms}–V_{rms}–L_{rms} characteristics (Figure 4g), the TiO$_2$ electrode decreased the turn-on voltage from 2.18 to 1.44 V. The maximum luminance values measured at the front of the device (ITO side) and at the back of the device (TiO$_2$ side) were 2260 and 1530 cd m^{-2}, respectively, resulting in a total luminance of 3790 cd m^{-2}. Here, backscattering of light by the TiO$_2$ layer resulted in a higher outcoupling of light through the ITO side than the TiO$_2$ side. Such high luminance is unprecedented for ECLDs and is achieved here because the large contact area of the TiO$_2$ electrode promotes the redox reaction of TAPC and TPBi, which are both present at high concentrations. This avoids the generation of vulnerable TBRb ions, thus preventing breakdown of the device. In addition, light scattering by the TiO$_2$ electrode likely improves the light outcoupling efficiency through the front and back of the device. The maximum luminous efficacy was 2.06 lm W^{-1} for forward emission and 3.71 lm W^{-1} when considering the total emission (Figure 4h, statistics of device performance in Figure S3, Supporting Information). The lifetime under continuous operation with the 300 Hz sinusoidal signal was 312, 195, and 138 s for an initial luminance of 300, 500, and 1000 cd m^{-2} at the front of the device, respectively; the resulting acceleration factor was 0.667 (Figure 4i; luminance decay over time data is shown in Figure S6, Supporting Information). Thus, the use of the TiO$_2$ electrode improved the operational lifetime by about one order of magnitude compared to the ex-ECLD without a TiO$_2$ electrode.

3. Conclusion

We developed and presented ex-ECLDs that operate based on an exciplex formation pathway, and demonstrated significant improvements in luminance, luminous efficacy, and operational lifetime compared to ECLDs based on the conventional annihilation pathway. Exciplex formation was confirmed to occur in a concentrated solution of TAPC and TPBi using transient PL spectroscopy. The addition of TBRb at 3×10^{-2} M resulted in complete energy transfer from the exciplex to TBRb. This operating mechanism separates the process of ionization-recombination (occurring on TAPC and TPBi) from the emission process (facilitated by TBRb), and therefore increases the efficiency and robustness of the ECL reaction. The application of a mesoporous TiO$_2$ electrode led to a further significant improvement in the performance of our ex-ECLDs. An optimized ex-ECLD with a TiO$_2$ electrode achieved a very high luminance of 3790 cd m^{-2} and a half-life of 312 seconds at an initial brightness of 300 cd m^{-2}. Unlike for most conventional OLEDs, the luminous efficacy of our ex-ECLDs increased with increasing device luminance since the

rate of ion collision is proportional to the square of the ion concentration in the device. An interesting implication of this effect is that the acceleration factors for the operational lifetime of our ex-ECLDs are less than 1.

In the future, the application of exciplexes in ECLD could be extended to devices with green or blue emission by the development of a higher-energy exciplex from a donor–acceptor combination with a larger energy LUMO–HOMO gap. However, in our work, we observed that the TAPC:TPBi exciplex showed a lower energy in solution than in a thin film, and this energy reduction in solution will need to be overcome to develop high-energy exciplex systems. While our results demonstrate that the exciplex pathway can drastically improve the performance of ECLDs, practical applications will likely require further advances in performance. Future developments of ECLD technology could benefit from the use of high-performance organic compounds that were originally developed for OLEDs and that can likely be used in ECLDs, possibly with minor modifications to improve solubility. In this context, a promising opportunity could be the selection of dyes that sensitize triplet states, i.e., phosphorescent and TADF dyes. In this study, we used a fluorescent dye and did not detect triplet sensitization by the exciplex intermediate, possibly because – in solution – the FRET rate is much faster than the intersystem crossing rate of the exciplex. Optimization of the solvent to maximize exciplex formation provides another opportunity. We found that the use of acetonitrile in our devices reduces the relative emission intensity of the TAPC:TPBi exciplex (Figure S7, Supporting Information). Thus, identification of a pair of polar and non-polar solvents that do not interrupt the exciplex formation will further improve the ECL reaction. Moreover, to increase the operational lifetime of the device, modification of the AC driving conditions, e.g., the introduction of a voltage offset, may help to balance the ion concentrations and prevent side reactions.

4. Experimental Section

Materials: TAPC, TCTA, and TBRb with 99% or higher purity were obtained from Luminescence Technology Corp. Tetrabutylammonium hexafluorophosphate, anatase TiO$_2$, a surfactant (Triton X-100), polystyrene microbeads, anhydrous toluene, and anhydrous acetonitrile were purchased from Merck KGaA. Rectangular glass substrates (15 mm × 24 mm × 0.7 mm) precoated with two 100 nm thick strips of ITO (2 mm × 22 mm each) were purchased from Xinyan Technology Ltd. UV-curable NOA68 and 3035BT resins were purchased from Norland Products and Threebond International, respectively.

Optical Characterization: The optical properties of the solutions were analyzed using 700 µL quartz cuvettes. The PL spectra and transient PL of the solutions were analyzed using a fluorescence lifetime spectrometer (FluoTime 250, PicoQuant) coupled with a picosecond diode laser ($\lambda = 373$ nm). UV–Vis–NIR absorption measurements of the solutions were carried out using a spectrophotometer (Cary 50 Bio, Varian). The total transmittance of the TiO$_2$ layer coated on a glass substrate was analyzed using a spectrophotometer (Lambda 1050, PerkinElmer) equipped with an integrating sphere.

Device Fabrication: The device fabrication is illustrated in Figure S8, Supporting Information. Each ECLD was fabricated from a pair of rectangular ITO-coated glass substrates. The substrates were cleaned thoroughly using a detergent solution (2% Hellmanex III in Milli-Q water), acetone, and isopropyl alcohol in a wet deck. After drying the substrates, the surface of ITO was treated with UV-ozone for 10 min, then a TiO$_2$ electrode

**ADVANCED
SCIENCE NEWS**

www.advancedsciencenews.com

**ADVANCED
MATERIALS**

www.advmat.de

was coated onto one of the substrates if required (see below). Polystyrene microbeads with a diameter of 30 µm were mixed with NOA68 resin. Small droplets of the resin were applied to the edges and corners of one of the ITO substrates, as shown in Figure S8, Supporting Information. The other substrate was placed over the first ITO substrate at a 90° angle, thus creating four regions where the ITO stripes cross and forming active areas with a size of 4 mm^2 where the ITO electrodes from each substrate face each other. The substrates were pressed together using a custom-made holder and the resin was cured using a UV lamp. This procedure yielded a tightly bonded pair of substrates with a gap of 30 µm that is set by the diameter of the polystyrene beads (Figure S9, Supporting Information). The bonded substrates were then transferred to a nitrogen-filled glove box and 50 µL of the ECL solution was pipetted into the gap between ITO substrates to fill the structure. Finally, 3035BT resin was applied and cured using a UV lamp to seal the edges.

Application of the TiO$_2$ Electrode: 2 g of anatase TiO$_2$ nanopowder (< 25 nm particle size), 8 mL of water, 1.6 mL of acetylacetone, and 0.1 mL of Triton X-100 were mixed in a vial and stirred to form a paste. The TiO$_2$ electrodes were formed by a sol–gel process with blade coating in a well-ventilated fume hood (schematics in Figure S10, Supporting Information). Briefly, stripes of 69 µm thick polyimide tape (Kapton, 3M) were applied to ITO-coated glass substrates, then 0.2 mL of the paste was applied onto the substrate and spread with a glass slide. The substrates were left in the fume hood for 15 min to allow the solvent to evaporate, then the polyimide tapes were removed and the substrates were transferred to a hot plate. The substrates were annealed at 300°C for 3 h. This process forms a 32 µm thick mesoporous TiO$_2$ electrode.

Device Characterization: A schematic of the device characterization setup is depicted in Figure S11, Supporting Information. The sample was placed in the center of a 55 cm × 55 cm dark box. A function generator (33220A, Agilent Technologies) providing square or sinusoidal signals of variable amplitude and frequency was used to drive the ECLDs. A power analyzer (GPM-8213, GW Instek) was utilized to monitor the actual V_{rms} and I_{rms} applied to the devices. The light intensity was measured with a silicon photodiode (PDA100A2, Thorlabs) placed 168 mm away from the active device area. The rms of the photodiode voltage was monitored by a multimeter (Keithley 2100, Keithley Instruments) operating in AC mode. Spectral data was collected using a fiber-coupled spectrometer (Ocean HDX, Ocean Insight). All components were connected to a computer running custom software to automatize the measurement of voltage–current–luminance and frequency-luminance characteristics, as well as the operational lifetime measurements. A latency time of 0.4 ms was used between datapoints in scans of voltage and frequency. A Lambertian emission pattern was assumed to calculate the luminous flux from each ECLD. To measure the operational lifetime, the rms of the photodiode voltage was monitored while continuously operating the device with a sinusoidal voltage. To characterize transients, an oscilloscope was connected to the setup in place of the multimeter and the waveform analyzer.

Supporting Information

Supporting Information is available from the Wiley Online Library or from the author.

Acknowledgements

Conflict of Interest

The authors declare no conflict of interest.

Data Availability Statement

The data that support the findings of this study are openly available in University of St Andrews at https://doi.org/10.17630/211d7176-e99d-45fe-8cd7-db7e9b2dfcf4.

Keywords

[1] a) S.-C. Chang, Y. Yang, Q. Pei, *Appl. Phys. Lett.* **1999**, *74*, 2081; b) S.-C. Chang, Y. Yang, *Appl. Phys. Lett.* **1999**, *75*, 2713; c) S. H. Kong, J. I. Lee, S. Kim, M. S. Kang, *ACS Photonics* **2017**, *5*, 267; d) K. G. Cho, J. I. Lee, S. Lee, K. Hong, M. S. Kang, K. H. Lee, *Adv. Funct. Mater.* **2020**, *30*, 1907936. e) P. McCord, A. J. Bard, *J. Electroanal. Chem.* **1991**, *318*, 91.

[2] a) C. A. Marquette, L. J. Blum, *Anal. Bioanal. Chem.* **2008**, *390*, 155; b) M. Zhang, L. Ge, S. Ge, M. Yan, J. Yu, J. Huang, S. Liu, *Biosens. Bioelectron.* **2013**, *41*, 544; c) K. Muzyka, *Biosens. Bioelectron.* **2014**, *54*, 393; d) S. E. Kirschbaum, A. J. Baeumner, *Anal. Bioanal. Chem.* **2015**, *407*, 3911; e) W. Gao, M. Saqib, L. Qi, W. Zhang, G. Xu, *Curr. Opin. Electrochem.* **2017**, *3*, 4; f) M. Chen, Z. Ning, K. Chen, Y. Zhang, Y. Shen, *J Anal Test* **2020**, *4*, 57.

[3] a) M. Bhaiyya, P. K. Pattnaik, S. Goel, *Curr. Opin. Electrochem.* **2021**, *30*, 100800; b) T. Kasahara, S. Matsunami, T. Edura, R. Ishimatsu, J. Oshima, M. Tsuwaki, T. Imato, S. Shoji, C. Adachi, J. Mizuno, *Sens. Actuators, A: Phys.* **2014**, *214*, 225.

[4] a) K. Nishimura, Y. Hamada, T. Tsujioka, S. Matsuta, K. Shibata, T. Fuyuki, *Jpn. J. Appl. Phys.* **2001**, *40*, L1323; b) H. C. Moon, T. P. Lodge, C. D. Frisbie, *Chem. Mater.* **2014**, *26*, 5358; c) H. C. Moon, T. P. Lodge, C. D. Frisbie, *J. Mater. Chem. C* **2016**, *4*, 8448; d) S. Tsuneyasu, K. Ichihara, K. Nakamura, N. Kobayashi, *Phys. Chem. Chem. Phys.* **2016**, *18*, 16317; e) A. Abdussalam, G. Xu, *Anal. Bioanal. Chem.* **2022**, *414*, 131.

[5] a) T. Nobeshima, T. Morimoto, K. Nakamura, N. Kobayashi, *J. Mater. Chem.* **2010**, *20*, 10630; b) T. Nobeshima, K. Nakamura, N. Kobayashi, *Jpn. J. Appl. Phys.* **2013**, *52*, 05DC18; c) H. Oh, Y. M. Kim, U. Jeong, H. C. Moon, *ChemElectroChem* **2018**, *5*, 2836; d) L. C. Soulsby, E. H. Doeven, T. T. Pham, D. J. Eyckens, L. C. Henderson, B. M. Long, R. M. Guijt, P. S. Francis, *Chem. Commun.* **2019**, *55*, 11474.

[6] a) S. Tsuneyasu, T. Ichikawa, K. Nakamura, N. Kobayashi, *ChemElectroChem* **2017**, *4*, 1731; b) E.-S. Ko, J. I. Lee, H. C. Lim, J.-E. Park, S. H. Kong, J.-I. Hong, M. S. Kang, I.-S. Shin, *ACS Photonics* **2018**, *5*, 3723; c) H. Hwang, J. K. Kim, H. C. Moon, *J. Mater. Chem. C* **2017**, *5*, 12513.

[7] a) Y. S. Park, S. Lee, K. H. Kim, S. Y. Kim, J. H. Lee, J. J. Kim, *Adv. Funct. Mater.* **2013**, *23*, 4914; b) J. H. Lee, S. Lee, S. J. Yoo, K. H. Kim, J. J. Kim, *Adv. Funct. Mater.* **2014**, *24*, 4681; c) M. Sarma, K.-T. Wong, *ACS Appl. Mater. Interfaces* **2018**, *10*, 19279.

[8] a) M. Colella, A. Danos, A. P. Monkman, *J. Phys. Chem. Lett.* **2019**, *10*, 793; b) H. Nakanotani, T. Furukawa, K. Morimoto, C. Adachi, *Sci. Adv.* **2016**, *2*, e1501470.

[9] B. S. Kim, J. Y. Lee, *Adv. Funct. Mater.* **2014**, *24*, 3970.

[10] K. Goushi, K. Yoshida, K. Sato, C. Adachi, *Nat. Photonics* **2012**, *6*, 253.

[11] J. I. Lee, D. Kang, S. H. Kong, H. Gim, I.-S. Shin, J. Kim, M. S. Kang, *ACS Appl. Mater. Interfaces* **2018**, *10*, 41562.

[12] a) B. O'Regan, M. Grätzel, *Nature* **1991**, *353*, 737; b) S. Okamoto, K. Soeda, T. Iyoda, T. Kato, T. Kado, S. Hayase, *J. Electrochem. Soc.* **2005**, *152*, A1677; c) T. Kado, M. Takenouchi, S. Okamoto, W. Takashima, K. Knateo, S. Hayase, *Jpn. J. Appl. Phys.* **2005**, *44*, 8161.